ELSEVIER

International Journal of Heat and Fluid Flow 22 (2001) 614–623

International Journal of HEAT AND FLUID FLOW

www.elsevier.com/locate/ijhff

Leading edge film cooling heat transfer with high free stream turbulence using a transient liquid crystal image method

S. Ou, R.B. Rivir *

Air Force Research Laboratory/PRTT, Propulsion Directorate, 1950 Fifth street, WPAFB, OH 45433-7251, USA

Received 23 October 2000; accepted 10 June 2001

Abstract

This paper studies film effectiveness and heat transfer coefficients on a large scale symmetric circular leading edge with three rows of film holes. The film hole configuration focuses on a smaller injection angle of 20° and a larger hole pitch with respect to the hole diameter ($P/d = 7.86$). The study includes four blowing ratios ($M = 1.0, 1.5, 2.0$ and 2.5), two Reynolds numbers ($Re = 30{,}000$ and 60,000), and two free stream turbulence levels (nominally $Tu = 1\%$ and 20% depending on the Reynolds number). A transient liquid crystal (LC) image technique is employed to obtain the film effectiveness and heat transfer coefficient distributions with high spatial resolutions of 0.6 mm in both streamwise and spanwise directions. Results are presented for detailed and spanwise averaged values of film effectiveness and Frössling number. Turbulence intensity has an attenuation on film effectiveness as well as on Frössling number for all blowing ratios at $Re = 30{,}000$. Under high turbulence conditions the film effectiveness and Frössling number increase as blowing ratio increases from 1.0 to 2.0 for both Reynolds numbers. Further increasing the blowing ratio results in reverse effect. Increasing the Reynolds number from 30,000 to 60,000 results in increases in both the film effectiveness and Frössling number at high turbulence except for $M = 2.5$. The blowing ratio of two shows a spatial coupling of the stagnation row of film holes with the second row (21.5°) of film holes which results in the highest film effectiveness and also the highest Frössling numbers.

Keywords: Leading edge; Film cooling; Film effectiveness; Frössling number; Heat transfer coefficient; Turbulence; Transient; Liquid crystal; Blowing ratio; Reynolds number

1. Introduction

As the high performance turbine engine technologies advance, the turbine inlet temperature is raised to higher levels to achieve higher thermal efficiency. Current material technologies require film cooling to protect the turbine airfoils from the hot gas stream, especially the leading edge due to its exposure to the highest temperatures. Minimizing the amount of coolant used in the film cooling requires consideration of techniques to extend the area of film coverage such as the injection angle and the film hole pitch. Extending the coolant to cover more spanwise and streamwise areas by reducing the injection angle and adjusting the blowing ratio, the hole pitch may be increased thus reducing the number of required film holes. This can also increase the strength of the airfoil due to the reduction in the number of film holes.

In the past, many leading edge film cooling studies have used large injection angles (30°–35°) and small hole pitch (3–4 injection hole diameters). Mick and Mayle (1988) performed tests using a blunt body with a circular leading edge and a flat afterbody to study the detailed film effectiveness and heat transfer coefficients for secondary air injection through three rows of holes (located at ±15° and +44°) into the stagnation region of an incident mainstream flow. The holes in each row were spaced four-hole diameters apart and were angled 30° to the surface in the spanwise direction. At a low mainstream turbulence they found that large spanwise variations exist in both film effectiveness and heat transfer coefficient. They also reported that the highest values of film effectiveness and heat transfer coefficient do not occur at the same location. Mehendale and Han (1992) and Ou et al. (1992) used a similar test model as that of Mick and Mayle to study the effect of the high mainstream turbulence on leading edge film cooling and heat transfer at a Reynolds number of 100,000. They also used a spanwise injection angle of 30° but a hole pitch of three-hole diameters. Mehendale and Han found that for a two-row injection at ±15° and ±40° the film effectiveness for a blowing ratio of 0.4 is significantly reduced by high mainstream turbulence, but the effect is diminished for blowing ratios of 0.8 and 1.2 and that the heat transfer coefficient for a blowing ratio of 0.8 increases with increasing mainstream turbulence,

* Corresponding author. Fax: +1-937-656-4531.

E-mail addresses: shichuan.ou@wpafb.af.mil (S. Ou), richard.rivir@wpafb.af.mil (R.B. Rivir).

0142-727X/01/$ - see front matter
PII: S0142-727X(01)00121-7

Notation

b	diameter of blown grid tube, 15.88 mm
c_p	specific heat, kJ/kg °C
d	film hole diameter, 4.76 mm
D	leading edge diameter, 8.89 cm
h	heat transfer coefficient
k	thermal conductivity, W/m °C
M	blowing ratio, $\rho_c U_c/\rho_\infty U_\infty$
N	number of steps
Nu	Nusselt number, hD/k
P	hole pitch, the distance between same row hole centers
Re	Reynolds number based on leading edge diameter, D
t	time, s
T	temperature, °C
Tu	free stream turbulence intensity
U	unit function (in Eqs. (8)–(11))
U_c	coolant velocity, m/s
U_∞	free stream velocity, m/s
x	streamwise distance from blown grid coordinate perpendicular to the surface
X	surface distance from the stagnation line
Z	spanwise (lateral) coordinate
Λ	integral scale of turbulence
α	thermal diffusivity, m^2/s
δ	boundary layer thickness
λ	micro scale of turbulence
η	film effectiveness
ρ_∞	free stream density, kg/m^3
ρ_c	coolant density, kg/m^3

Subscripts

c	coolant
f	film
i	initial
m	mainstream
w	wall

but the effect is not consistent for blowing ratios of 0.4 and 1.2. Similarly, Ou et al. also pointed out that for a one-row injection at ±15° the mainstream turbulence adversely affects the film effectiveness for a blowing ratio of 0.4 but the effect is reduced for blowing ratios of 0.8 and 1.2 and that the heat transfer coefficient increases with mainstream turbulence levels for blowing ratios of 0.4 and 0.8, but the effect is not systematic for the blowing ratio of 1.2. Ekkad et al. (1995) studied the effect of free stream turbulence on the detailed distributions of film effectiveness and heat transfer coefficient on a cylindrical leading edge model using a transient liquid crystal (LC) image method. Again, an injection angle of 30°, a pitch of four-hole diameters, and a hole row location at ±15° were used in this study. They found that the heat transfer coefficient increases with an increased blowing ratio but the film effectiveness reaches a peak value at blowing ratio of 0.4. Their results also show that higher mainstream turbulence reduces the film effectiveness for lower blowing ratios but the effect diminishes at higher blowing ratios.

This investigation considers a blade injection angle of 20° and a pitch to hole diameter ratio of 7.86 to extend the film coverage over the larger injection angles and smaller pitch of film holes. Karni and Goldstein (1990) investigated a single row of 20° film holes with a P/d of 5.98 on a cylinder which was rotated to 0°, 7°, 10° and 30° for blowing ratios of 0.5–2.0 using a naphthalene mass sublimation technique to determine the local heat transfer coefficient distribution. Measurements of film effectiveness for a similar geometry to the one investigated in this study have been reported by Cruse et al. (1997). Cruse investigated a density ratio of 1.8 with a half plane simulation of the leading edge. Two rows of film holes are located at 0° and 25°. An infrared technique was used to measure the surface temperature distribution for the film effectiveness. Yuki et al. (1998) used same test rig as Cruse's to obtain the heat transfer coefficients by means of a thin film constant heat flux technique. Computations for the Cruse geometry have been preformed and reported by Martin and Thole (1997), Thakur et al. (1997), Lin et al. (1997), and Chernobrovkin and Lakshminarayana (1999). The comparisons of the computations with the experiment showed good agreement for the film effectiveness. Chernobrovkin has observed the turbulence length scale has such an effect on the computation that it is impractical to attempt a calculation at $Tu = 20\%$. To improve the measurement accuracy of the heat transfer coefficient Yuki et al. (1998) investigated the density ratio of 1.1 for the same experiments of Cruse but without a direct determination of the film effectiveness for all cases. In the Yuki experiment, the film holes were found to locally distort the electric field generated on the constant heat flux surface which in turn resulted in distortion in the local heat transfer coefficient. Mick and Mayle (1988) noticed the same problem and applied a correction to determine the local heat flux. Yuki presents the heat transfer coefficients as a ratio of the cooled to the uncooled value to remove the distortion effect. Significant increases in the heat transfer coefficients with film cooling observed by Cruse, Yuki, and the earlier experiments are of course a significant concern to accurately determine the net heat load to the turbine airfoils.

The transient LC method employed in this effort provides both the film effectiveness and the heat transfer coefficient from two sets of measurements on the same configuration with the same thermal boundary conditions which are solved simultaneously. The effects of large values of curvature, pressure gradient, combined with high free stream turbulence at a nominal density ratio of 1.0 are the subjects of this investigation. Two turbulence levels, two Reynolds numbers, and four blowing ratios are investigated and the resulting heat transfer coefficient and the film effectiveness reported.

2. Test facility

The facility shown schematically in Fig. 1 consists of a 76.2 cm diameter settling chamber with a 30.5 cm diameter solenoid valve to switch the primary temperature-controlled flow from a bypass loop to the test loop. A secondary temperature-controlled turbulence flow loop and a third temperature-controlled film flow (coolant flow) loop with manual valves complete the flow path. All temperature-controlled loops are capable of both heating and cooling. The test article with a height of 36.4 cm is a full half cylinder joined by a flat afterbody. There are three rows of film holes located, respectively, at the stagnation line and ±21.5° from the stagnation line. The film holes located at ±21.5° row are staggered with respect to those at stagnation row. Each film hole is spanwise spaced 7.86 hole diameters apart. The holes are angled 20° and 90 to surface in the spanwise and streamwise directions. The hole to

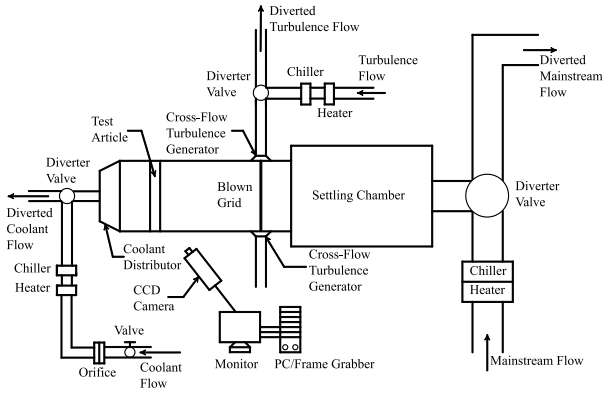

Fig. 1. Schematic of test facility.

leading edge diameter ratio is 0.054 and the hole length to hole diameter ratio is 11.69. Nine locations of hot wire traverse stations for the approaching flow profile measurements are provided along the centerline on the top wall.

The turbulence generator consists of a blown grid plus jets in cross flow to achieve high turbulence intensity and uniform velocity and turbulence profiles over the test section. The blown grid and the cross-flow jet are in the same plane which is located at 118.9 cm upstream of the stagnation line of the test article location ($x/b = 74.9$). Typical velocity profiles show uniformity of 1–2% over the film measurement area at both low (about 1%) and high turbulence (about 20%) levels. The midspan centerline velocity and turbulence intensity distributions are shown in Fig. 2. The midspan centerline velocities

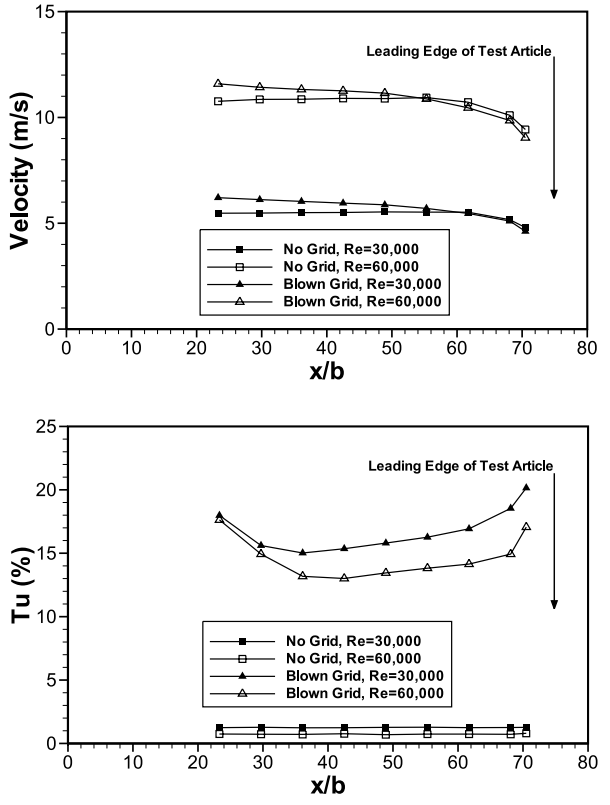

Fig. 2. Midspan centerline velocity and turbulence intensity distributions.

show similar trends at both Reynolds numbers. The blown grid initially has higher velocity than the no grid case. This is likely due to the nonuniform mixing between the mainstream flow and the strong jets from the blown grid and the cross flow turbulence generator. As the mixing flow continues downstream, the difference between the velocities reduces gradually until it is within 4% at the location of 6.99 cm upstream of the stagnation. The blown grid turbulence initially decays with x just like a traditional grid until $x/b = 36.1$, where the turbulence starts to increase slightly. As the test article is approached, an increase in turbulence occurs due to the turning of the flow which reduces the axial measured component of velocity. Integral turbulence scales measured by correlation are typically the order of 3 cm ($\Lambda/d = 6.3$) at the test article for the high turbulence conditions.

3. Instrumentation and calibration

A wide band LC is used to measure the surface temperature of the test surface. A steady state hue calibration is initially carried out on a flat strip sprayed with the batch of LC used on the test article. The initial LC hue calibration is against a linear array of 19 thermocouples on a water-cooled and heated aluminum block which provides a linear distribution of temperature to calibrate the hue against temperature. The wide band LC used in the present study is BM/R38C5W/C17-10. The temperature calibration for this particular liquid crystal is 38.3, 39.1 and 43.8 °C for the red, green and blue hues, respectively. A second calibration is superimposed upon the original LC calibration to account for the test article's different illumination angles, camera view angle, and the curvature of the model. This calibration is accomplished by an in place measurement on the test article. A 2.54 cm wide by 0.05 mm thick stainless steel foil, constant heat flux surface, with 8 thermocouples distributed around a 90° segment is located on the model below the film cooling holes. This calibration strip is also coated with the same batch of LC to provide a direct in place calibration. A Sony XC-003 three-chip color CCD camera is used to acquire and transfer LC images. The raw data was acquired with a hue system originally developed by Farina and Moffat (1994) at Stanford University utilizing a Matrox frame grabber.

4. Theory of the transient LC technique

Transient heat transfer in a solid substrate coated with LC, which is suddenly exposed to a convective fluid at temperature $T_{m,}$ is governed by transient heat diffusion equation. Under the assumptions of 1D heat conduction (e.g., in the x direction) and without film injection, the local heat transfer coefficient, h, can be obtained by solving the following governing equation with the prescribed boundary conditions:

$$k\frac{\partial^2 T}{\partial x^2} = \rho c_p \frac{\partial T}{\partial t}, \tag{1}$$

where k is the thermal conductivity of solid, T the surface temperature, x the coordinate perpendicular to the surface (+ towards the inside of the solid), ρ the density of the solid, c_p the specific heat of the solid, and t is the time,

$$T(x,0) = T_i, \tag{2}$$

$$-k\frac{\partial T}{\partial x}\bigg|_{x=0} = h[T_m - T(0,t)], \tag{3}$$

$$T(\infty,t) = T_i. \tag{4}$$

The solution to Eq. (1) can be obtained in the form of the dimensionless temperature at the convective boundary surface (i.e., $x = 0$) as follows:

$$\frac{T_w - T_i}{T_m - T_i} = 1 - \exp\left[\frac{h^2 \alpha t}{k^2}\right] \operatorname{erfc}\left[\frac{h\sqrt{\alpha t}}{k}\right], \tag{5}$$

where T_w is the surface temperature, T_i the initial temperature, T_m the convective fluid temperature, and α is the thermal diffusivity of the solid.

For the situation with a single convecting fluid at temperature T_m, for example, a solid test surface coated with LC without film injection, the local heat transfer coefficient (h) can be obtained from Eq. (5) by knowing the initial temperature (T_i) of the test surface and the fluid flow temperature (T_m) and measuring the LC coated surface temperature indicated by the color display (T_w) at time (t).

In the film cooling application over a surface, however, there are three temperatures involved: the mainstream temperature T_m, the coolant temperature T_c, and the wall temperature T_w. For the film cooling case, the mainstream temperature T_m in Eq. (5) must be replaced by a film temperature T_f, which is the mixed temperature between the mainstream and coolant temperatures and governs the convection on the LC coated surface. Eq. (5) may be rewritten as

$$\frac{T_w - T_i}{T_f - T_i} = 1 - \exp\left[\frac{h^2 \alpha t}{k^2}\right] \operatorname{erfc}\left[\frac{h\sqrt{\alpha t}}{k}\right]. \tag{6}$$

To find the unknown T_f in terms of known quantities T_m and T_c, a dimensionless temperature is defined as the film effectiveness (η)

$$\eta = \frac{T_f - T_m}{T_c - T_m}$$

or

$$T_f = \eta(T_c - T_m) + T_m = \eta T_c + (1 - \eta) T_m. \tag{7}$$

Vedula and Metzger (1991) first introduced a technique to obtain the film effectiveness and heat transfer coefficient involving a three temperature, film cooling problem. Based on this approach, two separate but closely related tests are performed. In the first (cold) test, the mainstream is heated to the desired value depending on the liquid crystal in use while the coolant is slightly heated. In the second (hot) test, the mainstream and coolant are, respectively, heated to desired temperatures. In both tests the test article remains at room temperature. In the experiments, the true step changes in the applied fluid temperatures (both mainstream and coolant) are usually not possible and actually change with time. The actual time-dependent fluid temperature changes can be accounted for by modifying the equations using superposition and Duhamel's theorem with the fluid temperatures replaced by a series of steps. The solution of Eq. (6) is represented as

$$T_w - T_i = \sum_{j=1}^{N} U(t - \tau_j)(T_f - T_i)_j, \tag{8}$$

$$U(t - \tau_j) = 1 - \exp\left[\frac{h^2}{k^2}\alpha(t - \tau_j)\right] \operatorname{erfc}\left[\frac{h}{k}\sqrt{\alpha(t - \tau_j)}\right], \tag{9}$$

where T_f is time varying and unknown but related to the time variation in T_m and T_c and to the film cooling effectiveness. Substituting T_f from Eq. (7) into Eq. (8) and rearranging the equation, the final forms related to the respective first and second transient tests are

$$T_w - T_{i1} = \sum_{j=1}^{N_1} U(t - \tau_j)[(1 - \eta)(T_{m1} - T_{i1}) + \eta(T_{c1} - T_{i1})]_j, \tag{10}$$

$$T_w - T_{i2} = \sum_{j=1}^{N_2} U(t - \tau_j)[(1 - \eta)(T_{m2} - T_{i2}) + \eta(T_{c2} - T_{i2})]_j, \tag{11}$$

where N_1 and N_2 are the numbers of time steps to reach the detected temperature for the first and second transient tests, respectively. The two Eqs. (10) and (11) are solved to obtain the two unknowns, h and η for each pixel in the measurement region of interest.

5. Experimental procedure

The coolant flow temperature is measured by a thermocouple in the coolant chamber adjacent to a film hole. Air is used as film flow which results in a nominal density ratio of one, although the actual value varies between 1.02 and 1.06 during the transient test. The mainstream temperature is measured by a thermocouple in the plane of the stagnation line of the test article. The initial temperature of the test article is measured by a thermocouple attached to the outer surface on the flat afterbody. Another thermocouple attached on the inner surface of the coolant chamber is used to check the initial temperature and assure no gradient of temperature across the wall of the test article.

All the flows involved are initially diverted away from the test article by bypass loops. The flow temperatures are heated to the desired values and reach steady state during this period. A transient test is initiated by switching valves simultaneously with the test loop to force the mainstream flow, film flow and turbulence flow over the test article. The initiation of the transient test triggers a data acquisition system to record the mainstream flow and coolant flow temperatures. Two independent tests are performed for each case. The data will be reduced as described in the preceding section.

The leading edge is simulated by a full half cylinder joined by a flat afterbody of 20.32 cm in length. The test article made of acrylic plastic is 1.91 cm thick throughout in order to provide the required semi-infinite wall boundary condition. The measurement domain on the test surface is divided into 81 pixels streamwise and 138 pixels spanwise which cover two repeated hole cycles. The CCD camera records the LC images. The hue value of each pixel of each LC image is then converted into an array of temperatures. A Fortran program is used to solve simultaneously for the film effectiveness and heat transfer coefficient from Eqs. (10) and (11) at each pixel using the data from two temperature sets. The time for each pixel to reach a particular hue, a green hue in this case, is computed for each frame. The actual pixel representation on the surface or the local spatial resolution of h and η of the test article is about 0.6 mm in both streamwise and spanwise directions.

The major uncertainty in the transient LC measurement is contributed by the measured time for each pixel location to reach the particular color (temperature). The expected maximum error in time for the measured color change from frame to frame image is 0.5 s. The error associated with color calibration against temperature using thermocouples is estimated at 0.25 °C. Other uncertainty contributions include thermocouple measurements for mainstream and coolant temperatures, flow measurement to determine Reynolds number, blowing ratio and turbulence intensity, the test surface properties such as thermal conductivity, and thermal diffusivity,

and 3D conduction effect around the film holes. Taking these factors into account gives an uncertainty in h of 8.9% based on the odds of 20–1 and the method introduced by Kline and McClintock (1953). Since the heat transfer coefficient is first computed from Eqs. (10) and (11), the uncertainty of h is also involved in that of the Frössling number and film effectiveness. The resulting uncertainty of Frössling number is estimated to be 9.0%. The uncertainty in the film cooling effectiveness is estimated to be 10.9%.

6. Results and discussions

The detailed film effectiveness distribution of the measurement domain is shown in Fig. 3 for $Re = 60{,}000$, $M = 2.0$, $Tu = 0.7\%$ case. The total coolant flow rates are measured with an orifice plate meter. Individual periodic hole flow does not assure that the spatial flow is periodic. The LC measurements indeed indicate the flow accumulates from the lower spanwise film injection holes over the upper holes on the stagnation row. This is evidenced by the observation that the film effectiveness distribution of constant contours of 0.40 and 0.32 on the stagnation row increase at an angle of 6° toward the upper right as a result of the increasing spanwise flow. Coolant from the stagnation row flows mainly in the spanwise direction. Very little of the coolant is deflected in the streamwise direction by the mainstream flow because the mainstream velocity is very small around the stagnation line. This results in high levels of film effectiveness in the region between holes along the stagnation line. The film effectiveness decays gradually along the surface in the streamwise direction. Coolant from the 21.5° row holes is deflected immediately to the mainstream direction due to the much stronger mainstream velocity at this location. The distribution of film coverage is relatively narrow with large regions of low levels of film effectiveness between coolant streams. It is seen that the film effectiveness starts to rise at the region around the film hole, especially at the upstream and bottom edge of the film holes. The rising film effectiveness may be partially caused by 3D conduction effects around the film holes. Since the rise in film effectiveness is not symmetric, another contribution to these rising values may be coming from the induced horseshoe vortex system.

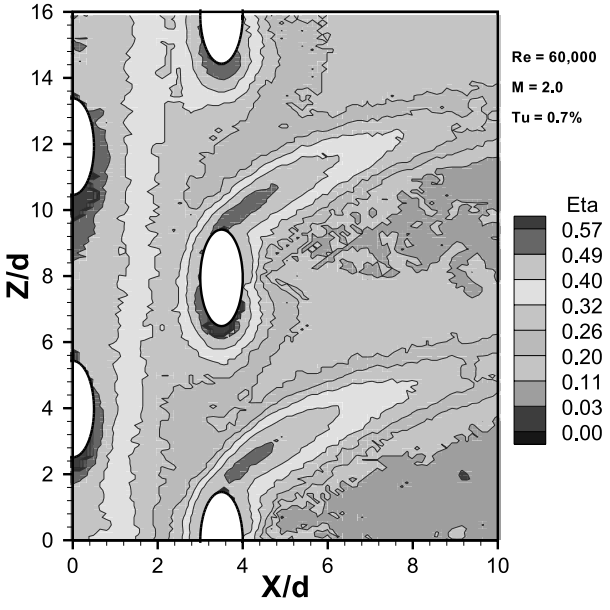

Fig. 3. Detailed film effectiveness distribution of measurement domain for $Re = 60{,}000$, $M = 2.0$, $Tu = 0.7\%$.

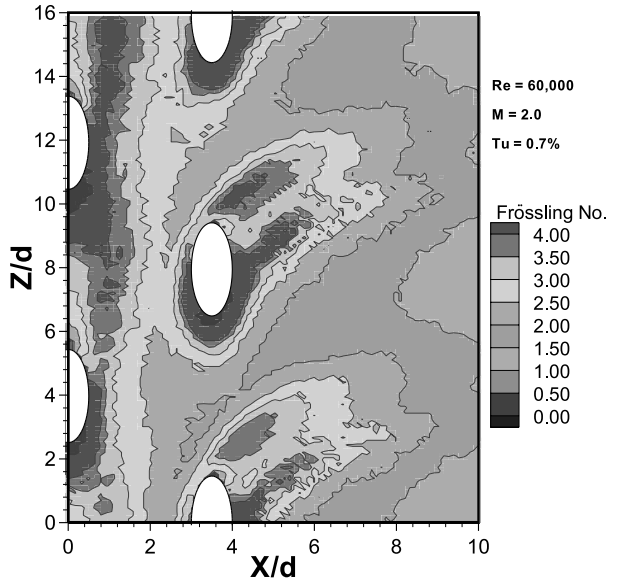

Fig. 4. Detailed Frössling number distribution of measurement domain for $Re = 60{,}000$, $M = 2.0$, $Tu = 0.7\%$.

Fig. 4 shows the detailed Frössling number distribution of the measurement domain for the corresponding case of film effectiveness. The Frössling number is defined as the Nusselt number divided by the square root of Reynolds number. Therefore it represents the heat transfer coefficient. The Frössling number distribution of constant contours (3.0 and 2.5) likewise shows a spanwise flow accumulation at the stagnation row. It is noted that the contours of the Frössling number are different from those of the film effectiveness. This agrees with the finding by Mick and Mayle (1988) that the highest values of film effectiveness and heat transfer coefficient do not occur at the same location. This finding was also confirmed by Yuki et al. This may also indicate that the characteristics of heat transfer coefficient are different from those of film effectiveness. The measurement domain covers two repeated hole cycles to check the periodicity. After the 21.5° row Figs. 3 and 4 indicate uniform periodicity in both film effectiveness and Frössling number distributions. The deviations of the two-hole cycle from periodicity range from 0.0% to ±28.1% (or ±0.03 out of 0.109) for film effectiveness, and 0 to ±18.2% (or ±0.52 out of 2.85) for Frössling numbers. The explanation of the coolant flow distribution as described in the film effectiveness in Fig. 3 in general applies to the trends of the Frössling number distribution.

The detailed distributions of film effectiveness and Frössling number are averaged (138 pixels) in the spanwise direction. It is noted that the LC data within the film holes is biased because it is actually not on the test surface. The computed spanwise averages have distorted the true values of heat transfer coefficients and film effectiveness at the hole locations. The spanwise averaged film effectiveness and Frössling numbers between film holes are therefore excluded from our plots as presented in the following figures.

6.1. Effect of turbulence intensity

Fig. 5 illustrates the spanwise averaged film effectiveness for $Re = 30{,}000$ at the two different turbulence levels for the four blowing ratios. As expected, the high free stream turbulence

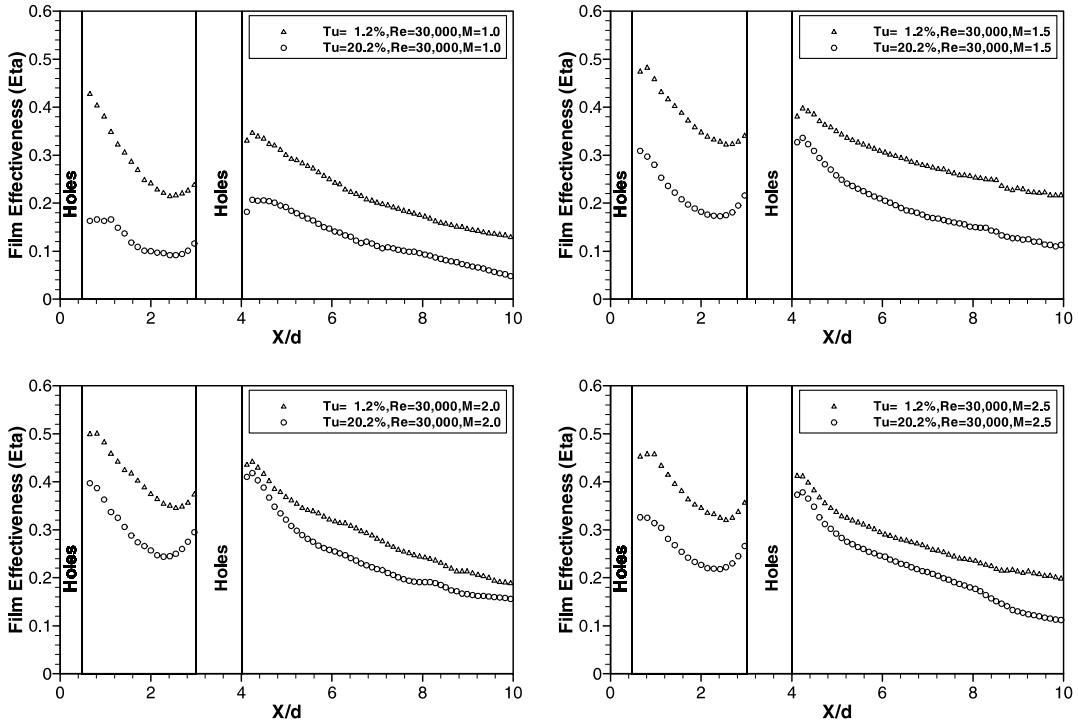

Fig. 5. Effect of turbulence on spanwise averaged film effectiveness for $Re = 30{,}000$ at four blowing ratios ($M = 1.0$, 1.5, 2.0 and 2.5).

reduces the film effectiveness for all blowing ratios at all locations. This is because the coolant jets are disturbed by the high free stream turbulence. Therefore the film coverage area is reduced (as observed in the course of experiment) and results in lower film effectiveness. The reductions are larger between the rows of film holes (61–20%) than downstream of the 21.5° row (46–21% at $X/d = 8$). The free stream turbulence has a more significant effect at lower blowing ratios of 1.0 and 1.5 than at higher blowing ratios of 2.0 and 2.5. The film effectiveness has a peak value near the downstream hole edge and decays along the surface in the streamwsie direction due to the dilution of the coolant flow. The film effectiveness starts to increase approximately 0.5 hole diameter upstream of the hole edge. Possible cause of this rise is explained in the discussion of the detailed film effectiveness distribution for Fig. 3.

Fig. 6 shows the spanwise averaged Frössling number for $Re = 30{,}000$ at two different turbulence levels for the four blowing ratios. Due to similar effect described in the preceding section the high free stream turbulence reduces the Frössling number distribution for all blowing ratios. However, the reductions are much smaller compared to the film effectiveness cases. The free stream turbulence has a more significant effect in the region between two rows (for example at $M = 2.5$, 17–21% vs. 3–19%) than the region after the 21.5° row for all blowing ratios.

6.2. Effect of blowing ratio

Fig. 7 shows the effect of blowing ratio on the spanwise averaged film effectiveness and Frössling number for $Re = 30{,}000$ and $Tu = 20.2\%$. At high turbulence, blowing ratio shows a strong effect on the film effectiveness between the rows. Both film effectiveness and Frössling number increase with increasing blowing ratio until it reaches 2.0. The blowing ratio of two provides the highest film effectiveness and Frössling number. If the blowing ratio is further increased to 2.5, both film effectiveness and Frössling number drop below the levels of blowing ratio 2.0. This may suggest a coolant lift-off from the test surface at the highest blowing ratio studied. The blowing ratio has more pronounced effect on the film effectiveness than on the Frössling number.

Fig. 8 presents the effect of blowing ratio on the spanwise averaged film effectiveness and Frössling number at $Re = 60{,}000$ and $Tu = 17.5\%$. Similar to the cases of $Re = 30{,}000$, both film effectiveness and Frössling number increase with increasing blowing ratio until the blowing ratio reaches 2.0. Further increasing the blowing ratio to 2.5 causes both the film effectiveness and Frössling number to drop dramatically to the levels of blowing ratio 1.5. This may also suggest a more severe coolant lift-off at the higher Reynolds number of 60,000 at the highest blowing ratio of 2.5. There exist only minor differences in both film effectiveness and Frössling number among $M = 1.0$, 1.5 and 2.5 for $0.5 < X/d < 3$ and $X/d > 5.8$.

6.3. Effect of Reynolds number

The effect of Reynolds number on the spanwise averaged film effectiveness for high turbulence case at four blowing ratios is presented in Fig. 9. As Reynolds number increases, the film effectiveness also increases for all blowing ratios. The trends show agreement with Mehendale and Han (1993) using thermocouple measurements. Reynolds number is seen to have a major effect only at the blowing ratio of $M = 1.0$. The effect diminishes as blowing ratio increases until there is virtually no effect for the $M = 2.5$ case for most of the locations. This may be due to the coolant lift-off as already discussed in Section 6.2.

Fig. 10 presents the effect of Reynolds number on the spanwise averaged Frössling number for high turbulence case at four blowing ratios. The Frössling number increases as Reynolds number increases with the exception of the highest blowing ratio, 2.5, which shows virtually no Reynolds number effect. This may be due to the more significant coolant lift-off. This may also reconfirm that the characteristics of heat

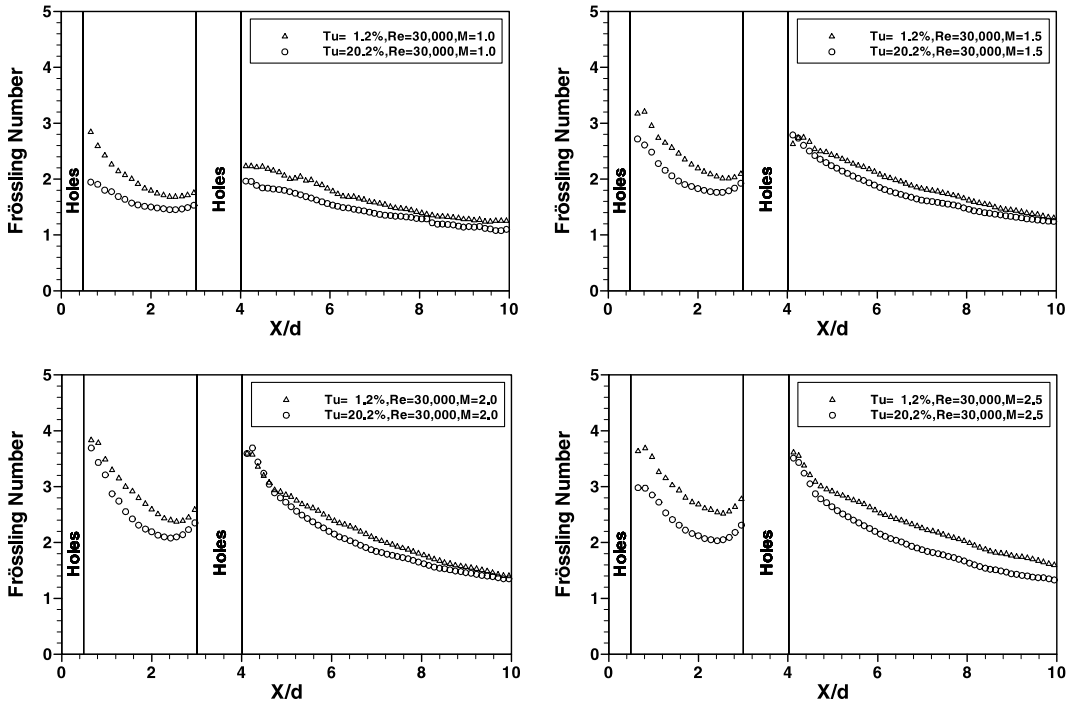

Fig. 6. Effect of turbulence on spanwise averaged Frössling number for $Re = 30{,}000$ at four blowing ratios ($M = 1.0$, 1.5, 2.0 and 2.5).

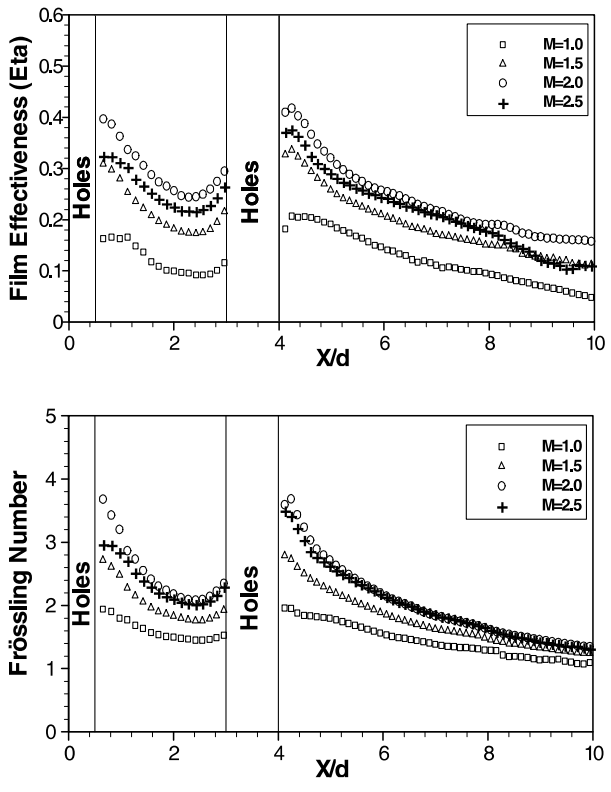

Fig. 7. Effect of blowing ratio on spanwise averaged film effectiveness and Frössling number for $Re = 30{,}000$ and $Tu = 20.2\%$.

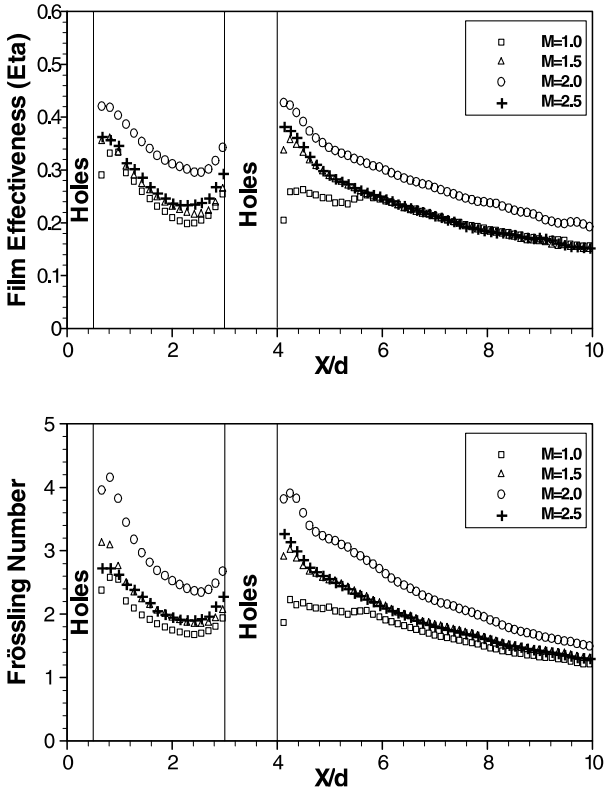

Fig. 8. Effect of blowing ratio on spanwise averaged film effectiveness and Frössling number for $Re = 60{,}000$ and $Tu = 17.5\%$.

transfer coefficient are different from those of film effectiveness. Although Frössling number has taken into account the square root of Reynolds number, there still exists an effect of Reynolds number. The results show the same trends with Mehendale and Han's study (1993), in which the Frössling number increases 19% after the first row and 21% after the

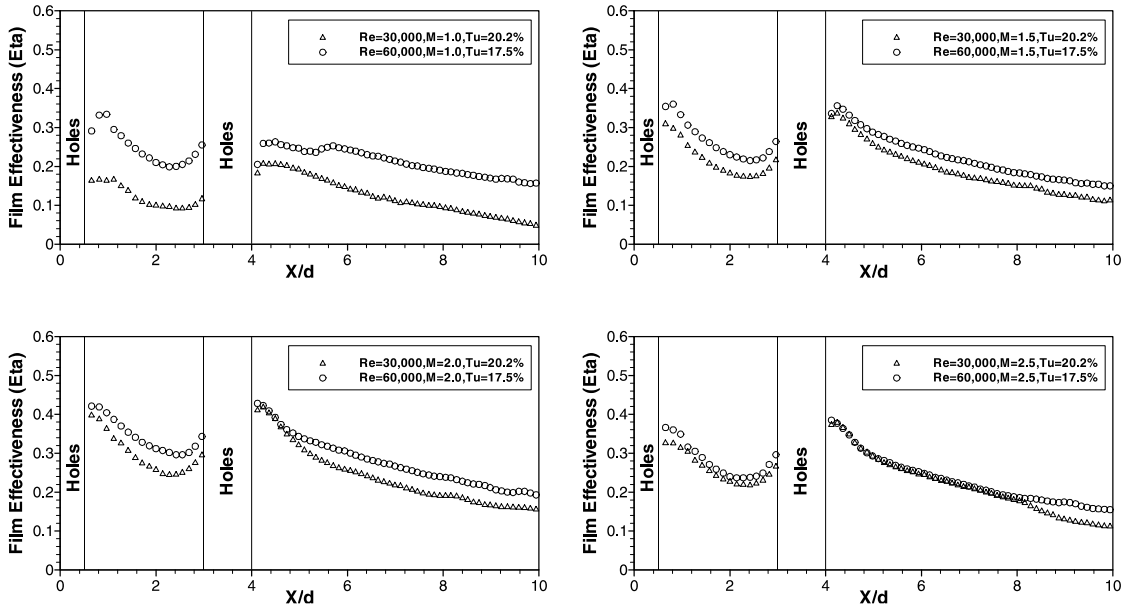

Fig. 9. Effect of Reynolds number on spanwise averaged film effectiveness for high turbulence at four blowing ratios ($M = 1.0$, 1.5, 2.0 and 2.5).

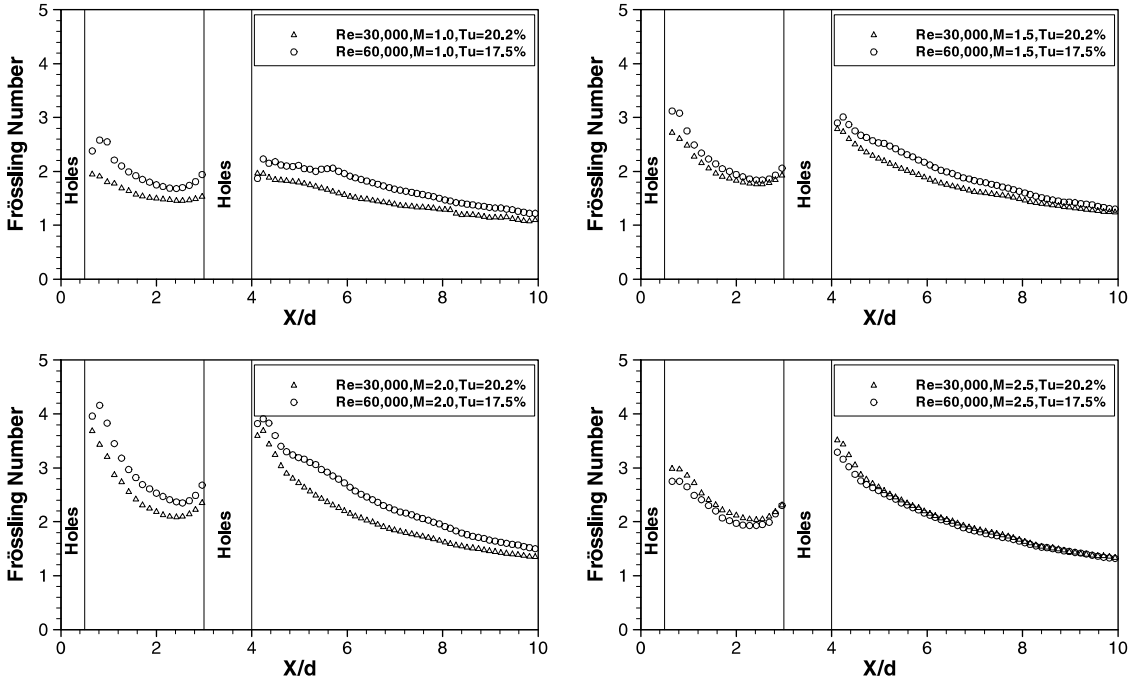

Fig. 10. Effect of Reynolds number on spanwise averaged Frössling number for high turbulence at four blowing ratios ($M = 1.0$, 1.5, 2.0 and 2.5).

second row for $M = 0.8$ as Reynolds number increases from 25,000 ($Tu = 8.53\%$) to 40,000 ($Tu = 7.59\%$). The Reynolds number is less significant on the Frössling number than it is on the film effectiveness.

6.4. The blowing ratio 2.0 case

In Fig. 4 the blowing ratio 2.0 case shows the coolant flow from the bottom hole on the stagnation row merges with that of the 21.5° row and extends over the 21.5° row (see the contour level of 2.50). A similar situation is also observed in Fig. 3 (see the contour level of 0.26). This allows coolant flow to be ingested by the 21.5° film holes to provide improved cooling from this row of holes. This would suggest that subtle adjustments of the relative positions of the stagnation row relative to the 21.5° row and blowing ratio could improve the performance with possibly a smaller cooling flow. Other blowing ratios show interactions of the two film rows as well but the $M = 2.0$ case illustrates the largest effects on the film effectiveness and Frössling number. This may also explain why

blowing ratio of 2.0 provides the highest film effectiveness and heat transfer coefficient for all locations.

6.5. Comparison with other results

The measured film effectiveness values are consistent with the experiments currently reported in the literature, Cruse et al. (1997) Yuki et al. (1998), and Reiss and Bölcs (1999), considering the differences in the experiments. The differences in the measured h values however remain significant. The parameter $Tu^*Re^{0.5}$ has been used by Smith and Kuethe (1966) and VanFossen and Ching (1994) for uncooled stagnation flows with success. The values of $Nu/Re^{0.5}$ normalized by the values from Smith and Kuethe have been plotted against $Tu^*Re^{0.5}$ for several experiments in Fig. 11(a) and (b) after the first row and after the second row of film holes, respectively. It is noted that the first and second row of film holes may not be at the same locations. This experiment shows agreement after the second row with Mehendale and Han (1993), the only experiment with a wide range of $Tu^*Re^{0.5}$, to better than 16%, with the exception of our $M = 2.0$ case, where strong coupling between the stagnation row and the 21.5° row was observed. The spread in the data after the first row of film holes is quite large as shown in Fig. 11(a). After the second row the spread collapses some but remains sizable. There are however similar slopes to our data, Mehendale and Han (1993), and Reiss and Bölcs (1999) with the Smith and Kuethe parameter of $Tu^*Re^{0.5}$. Comparison after second row with Yuki et al. (1998), a very similar experiment to the present one, indicates differences of −49% with Mehendale and Han's data and −56% from our data for h. While there are significant differences in flows, film hole configurations, boundary conditions and measurement techniques, these are not expected to account for the differences observed in h. The error estimates for all these experiments would seem to negate the possibility of the difference to be due simply to measurement errors. We have noted very strong interactions between the two rows of film holes. These interactions may be coupled with other flow and boundary-layer parameters. In the attempt to scale up the experiments to allow improved spatial resolution of the distributions of h and η experimenters are forced to address simulation of a number of parameters such as $D/\Lambda, d/\Lambda, d/\delta, \Lambda/\delta, /\delta, \lambda/\Lambda$, and Mach number. These parameters are normally thought to be secondary effects. When these effects are combined with some of the other variables of the problem they may become significant players, particularly in the leading edge problem. The integral (Λ) and micro scales (λ) of turbulence are examples of such a case. VanFossen and Ching (1994) has addressed the integral scale case without film cooling and proposed an empirical relationship with intensity and scale for the Frössling number which has a continual increase in h as the integral scale is decreased. Likewise it was pointed out by Chernobrovkin and Lakshminarayana (1999) that the turbulence scale interaction presents a problem for the computations as well. Since these measurements were taken we have improved both the spatial and temporal resolution by a factors of 12 or more. In making spot checks of the data with higher resolution measurements we believe what is presented to be accurate representation of a data set for this experiment.

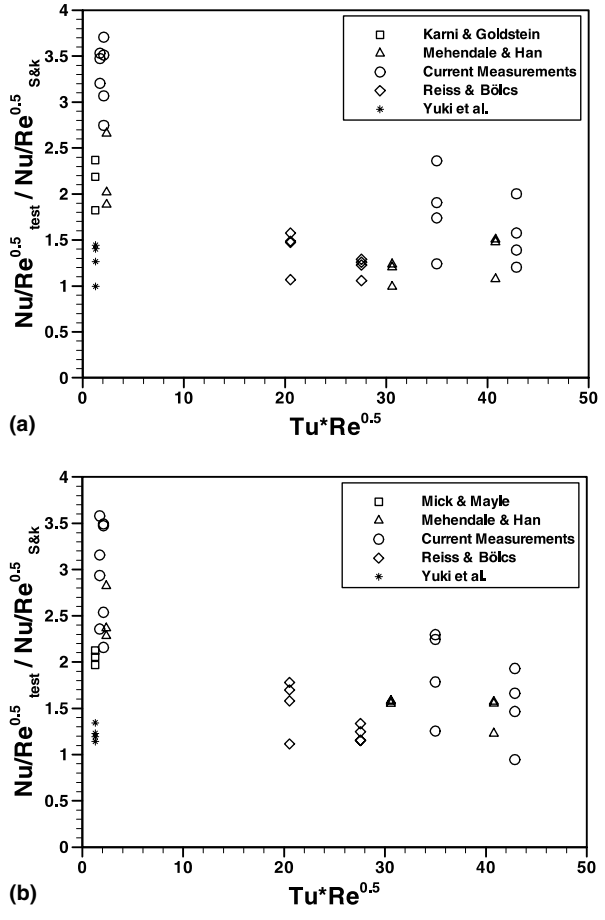

Fig. 11. Comparisons of heat transfer measurements with other results, heat transfer normalized by Smith and Huethe: (a) after first film row and (b) after second film row.

7. Summary and conclusions

High turbulence intensity results in film effectiveness attenuation of up to 61% between the rows for $Re = 30{,}000$. At the same Reynolds number, Frössling number is only weakly effected by turbulence. Blowing ratio has a very strong effect on film effectiveness between the rows at the high turbulence. The increases in the film effectiveness due to the blowing ratio range up to 2.8 times that for blowing ratio of 1.0. The $M = 2.0$ case consistently shows a coupling between the stagnation row and the 21.5° row resulting in the highest film effectiveness and Frössling number. The Reynolds number effect is most significant for the film effectiveness at all locations for the case of $M = 1.0$ and high turbulence. Both film effectiveness and Frössling number increase as a result of an increase in Reynolds number with an exception of $M = 2.5$ which shows virtually no effect of Reynolds number. Turbulence intensity, blowing ratio and Reynolds number are all equally important players in the effects on film effectiveness and heat transfer coefficient in the stagnation region. Since turbulence scale is a major effect in computations as well as experiments, its role in the stagnation film cooling problem should be further defined. The heat load ratios (ratio of heat flux with film injection to that without film injection) have been examined for several cases. A majority of locations (and thus the overall test surface) show a heat flux reduction due to the film flow. The film hole configurations in this research were used to match those of the F119 engine. The results of this research provided baseline aerothermal data for design and the calibration of computational codes used in the developments of the F119 engine in terms of the flow parameters studied such as Reynolds number, blowing ratio, and turbulence intensity.

Acknowledgements

This work was supported in part by Pratt and Whitney, and the Air Force Office of Scientific Research. Dr. Tom Beutner was the program manager. A part of this article was presented as ASME paper 2000-GT-0245; we acknowledge and appreciate permission from ASME to publish it.

References

Chernobrovkin, A., Lakshminarayana, B., 1999. Numerical simulation and aerothermal physics of leading edge film cooling. Proc. Inst. Mech. Eng. 213 (Part A), 103–118.

Cruse, M.W., Yuki, U.M., Bogard, D.G., 1997. Investigation of various parametric influences on leading edge film cooling. ASME Paper No. 97-GT-296.

Ekkad, S.V., Du, H., Han, J.C., 1995. Local heat transfer coefficient and film effectiveness distributions on a cylindrical leading edge model using a transient liquid crystal image method. ASME Winter Annual Meeting, San Francisco, CA.

Farina, D.J., Moffat, R.J., 1994. A system for making temperature measurements using thermochromic liquid crystals. Thermo Sciences Division, Stanford University, Report No. HMT-48.

Karni, J., Goldstein, R.J., 1990. Surface injection effect on mass transfer from a cylinder in crossflow: a simulation of film cooling in the leading edge region of a turbine blade. ASME J. Turbomachinery 112, 418–427.

Kline, S.J., McClintock, F.S., 1953. Describing uncertainties in single-sample experiments. Mech. Eng. January, 3–8.

Lin, Y., Stephenes, M.A., Shih, T.I-P., 1997. Computation of leading-edge film cooling with injection through rows of compound angle holes. ASME Paper No. 97-GT-298.

Martin, C.A., Thole, K.A., 1997. A CFD benchmark study: leading edge film-cooling with compound angle injection. ASME Paper No. 97-GT-297.

Mehendale, A.B, Han, J.C., 1992. Influence of high mainstream turbulence on leading edge film cooling heat transfer. ASME J. Turbomachinery 114, 707–715.

Mehendale, A.B., Han, J.C., 1993. Reynolds number effect on leading edge film effectiveness and heat transfer coefficient. Int. J. Heat Mass Transfer 36 (15), 3723–3730.

Mick, W.J., Mayle, R.E., 1988. Stagnation film cooling and heat transfer, including its effect within the hole pattern. ASME J. Turbomachinery 110, 66–72.

Ou, S., Mehendale, A.B., Han, J.C., 1992. Influence of high mainstream turbulence on leading edge film cooling heat transfer: effect of film hole row location. ASME J. Turbomachinery 114, 715–723.

Reiss, H., Bölcs, A., 1999. Experimental study of showerhead cooling on a cylinder comparing several configurations using cylindrical and shaped holes. ASME Paper No. 99-GT-123.

Smith, M.C., Kuethe, A.M., 1966. Effects of turbulence on laminar skin friction and heat transfer. Phys. Fluids 9 (12), 2337–2344.

Thakur, S., Wright, J., Shyy, W., 1997. Computation of a leading edge film cooling over an experimental geometry. ASME Paper No. 97-GT-381.

VanFossen, G.J., Ching, C.Y., 1994. Measurements of the influence of integral length scale on stagnation region heat transfer. NASA Technical Memorandum 106503.

Vedula, R.J., Metzger, D.E., 1991. A method for the simultaneous determination of local effectiveness and heat transfer distributions in three-temperature convection situations. ASME Paper No. 91-GT-345.

Yuki, U.M., Bogard, D.G., Cutbirth, J.M., 1998. Effect of coolant injection on heat transfer for a simulated turbine airfoil leading edge. ASME Paper No. 98-GT-431.